Raman Scattering and X-ray Diffraction Studies on Zinc(II) Bromide Solutions in Methanol and N,N-Dimethylformamide in the Temperature Range 77–333 K

Toshiyuki Takamuku*, Keisuke Nakamura, Mikito Ihara, Hisanobu Wakita, and Toshio Yamaguchi

Department of Chemistry, Faculty of Science, Fukuoka University, Nanakuma, Jonan-ku, Fukuoka 814-80, Japan

Z. Naturforsch. **49a**, 1119–1130 (1995); received October 15, 1994

Dedicated to Professor Hitoshi Ohtaki on the occasion of his 60th birthday

The structure of zinc(II) bromo complexes in methanol and N,N-dimethylformamide (DMF) (molar ratio [solvent]/[$ZnBr_2$] = 10, temperature range 77–333 K) has been investigated by Raman scattering and X-ray diffraction. In the methanol solution symmetric Zn–Br vibrations (ν_1) of the dibromo- and tribromozinc(II) complexes were observed at 209 and 184 cm^{-1}, respectively. With decreasing temperature the intensity of the ν_1 band decreased for the dibromo and increased for the tribromo complex. In addition, the ν_1 band for the tetrabromo complex appeared in the supercooled and glassy methanol solutions. In the DMF solution only one ν_1 band, assigned to both the dibromo- and tribromozinc(II) complexes, was observed. Its intensity did not change with temperature. The X-ray diffraction data revealed that the average number of Zn–Br interactions within the zinc(II) bromo complexes does not change with temperature while the number of nonbonding Br ··· Br interactions within the complexes increases from 1.5 at 298 K to 1.9 at 243 K for the methanol solution and from 1.3 at 298 K to 1.8 at 243 K for the DMF solution. These Raman and X-ray results have confirmed that in both methanol and DMF solutions at high temperatures the dibromo species is predominantly formed, whereas at low temperatures the tribromo complex is favored, the tetrabromo species being formed only in the supercooled and glassy methanol solutions. The temperature dependent equilibrium shifts of the zinc(II) bromo complexes in the methanol and DMF solutions are discussed together with previously reported results for the aqueous phase.

Key words: Raman spectroscopy, X-ray diffraction, Zinc(II) bromide, Methanol, N,N-Dimethylformamide.

1. Introduction

Knowledge of the molecular structure of electrolyte solutions in nonambient conditions such as the supercooled and glassy state or high temperatures and pressures is essential in understanding their physico-chemical properties and the chemical reactions taking place. We have investigated the structure of several aqueous electrolyte solutions in a wide temperature range by Raman spectroscopy, X-ray and neutron diffraction, and X-ray absorption spectroscopy [1–9]. Our previous Raman and X-ray studies [6, 7] on aqueous zinc(II) bromide solutions with [H_2O]/[$ZnBr_2$] molar ratios of 5 and 10 at temperatures from 77 to 413 K have revealed that the equilibria

$$3[ZnBr_2(OH_2)_2] + 2H_2O = 2[ZnBr_3(OH_2)]^- + [Zn(OH_2)_6]^{2+} \quad (1)$$

and

$$4[ZnBr_3(OH_2)]^- + 2H_2O = 3[ZnBr_4]^{2-} + [Zn(OH_2)_6]^{2+} \quad (2)$$

exist and shift to the right-hand-side when the temperature is lowered, the highest and lowest complexes, $[ZnBr_4]^{2-}$ and $[Zn(OH_2)_6]^{2+}$, being favored.

We discussed the equilibrium shifts in term of the ion–water and water–water bonding in the solutions. In supercooled and glassy aqueous zinc(II) bromide solutions, water molecules expelled from the first coordination shell of the dibromo and tribromo complexes are stabilized in reinforced hydrogen-bond networks, and thus a bromide ion binds more easily to a zinc(II) ion to form the tetrabromo complex at low temperature.

* On leave from Aqua Laboratory, Research and Development Division, TOTO Ltd., Nakashima, Kokurakita-ku, Kitakyushu 802, Japan.

Reprint requests to Prof. T. Yamaguchi.

0932-0784 / 94 / 1200-1119 $ 06.00 © – Verlag der Zeitschrift für Naturforschung, D-72027 Tübingen

From the above viewpoint of ion–solvent and solvent–solvent interactions it is interesting to examine the temperature influence on equilibria (1) and (2) in non-aqueous solvents such as methanol and DMF, in which the solvent–solvent interaction is weaker than in water. Methanol has the melting and boiling points m.p. = 175 K and b.p. = 338 K, and the donor and acceptor numbers DN = 19.0 and AN = 41.3. In addition, a methanol molecule has less hydrogen bonding sites than a water molecule. DMF has m.p. = 212 K, b.p. = 426 K, DN = 26.6 and AN = 16.0. An X-ray diffraction study on liquid DMF has revealed that DMF has a practically random structure [10, 11]. Therefore the solvent–solvent interaction in DMF is the weakest among the three solvents.

In the present study we have measured Raman spectra of zinc(II) bromide solutions in methanol and DMF with a [solvent]/[$ZnBr_2$] molar ratio of 10 in a wide temperature range from liquid nitrogen temperature (77 K) to 333 K. Furthermore, X-ray diffraction measurements on the same solutions have been performed at 243 and 298 K to determine the average structure of the complexes in the solutions. In combination with our previous results on the aqueous phase [6, 7], we discuss temperature-dependent equilibrium shifts of the zinc(II) bromide species on the basis of the ion–ion, ion–solvent, and solvent–solvent interactions.

2. Experimental

2.1 Reagents

All chemicals were of analytical reagent grade purchased from Wako Pure Chemicals.

Zinc(II) bromide (99.9%) and **Lithium bromide,** without further purification, were dried on P_2O_5 in a vacuum desiccator.

First, zinc(II) perchlorate hexahydrate was prepared from zinc(II) oxide and perchloric acid. The zinc(II) perchlorate thus prepared was recrystallized twice from water. **Zinc(II) perchlorate DMF solvates,** $Zn(ClO_4)_2(dmf)_x$, were then prepared by dissolving the zinc(II) perchlorate hexahydrate in DMF and recrystallized three times from DMF and finally from a DMF-acetone mixture. The crystals obtained were washed with diethyl ether and dried at 313 K in a vacuum oven after diethyl ether was vaporized off at room temperature. EDTA titrations showed that the crystals finally obtained are $Zn(ClO_4)_2(dmf)_6$.

Methanol was refluxed with some metal sodium tips for an hour and then distilled at ambient pressure.

DMF was dried for several days over molecular sieves 4A 1/16, and then distilled at 313 K under reduced pressure (270 Pa) with a small amount of calcium hydride.

2.2 Preparation of Sample Solutions

As methanol and DMF are hygroscopic, all sample solutions were prepared in a dry box under an atmosphere of dried nitrogen. The compositions of the sample solutions are given in Table 1. Solutions M2, D2(1) and D2(2) were prepared by dissolving dried zinc(II) bromide in distilled methanol or DMF to reach a [solvent]/[$ZnBr_2$] molar ratio of 10. Solution D1 was prepared by dissolving lithium bromide and the solvate in DMF, and solutions D3 and D4 by dissolving lithium bromide and zinc(II) bromide in DMF to required amounts. The concentrations of zinc(II) in the sample solutions were determined by titration with EDTA standard solution using Eriochrom Black T (EBT) as indicator. The concentrations of bromide were determined by gravimetry as AgBr. The densities of the solutions M2, D2(1), and D2(2) at 298 K were measured with a densitometer (ANTON Paar K.G.

Table 1. Concentrations, the molar ratios, densities ϱ at 298 K, and the stoichiometric volume V per zinc atom of the sample solutions.

Solution	M2	D0	D1	D2(1)	D2(2)	D3	D4
Zn^{2+}/mol kg^{-1}	2.903	0.4242	0.4848	1.350	1.295	1.522	1.283
Br^-/mol kg^{-1}	5.806		0.7063	2.700	2.590	4.517	4.931
$[Br^-]/[Zn^{2+}]$	2.000		1.457	2.000	2.000	2.968	3.843
$[CH_3OH]/[Zn^{2+}]$	10.75						
$[DMF]/[Zn^{2+}]$		32.25	28.22	10.13	10.22	8.990	10.66
ϱ/g cm^{-3}	1.174			1.169	1.167		
$V/10^8$ pm^3	8.060			13.72	13.84		

DMA 35), whereas those of the solutions M2 and D2(2) at 243 K were obtained by extrapolation of the densities measured in the temperature range 278–323 K with a densitometer (ANTON Paar K.G. DMA 602).

2.3 Raman Spectral Measurements

Each sample solution was sealed into a glass tube of 1.8 mm inner diameter. Raman scattering measurements were carried out for solution M2 at 166, 193, 213, 233, 253, 268, 298, 313, and 333 K, and for solution D2(1) at 153, 173, 193, 213, 233, 253, 268, 298, and 313 K with a Raman spectrometer (JEOL JRS-400T) using the 514.5 nm line from an argon ion laser (Spectra Physics Model 168B). Raman spectra of the solutions D0, D1, D3, and D4 were also recorded at 298 K. The temperature was measured with a copper-constantan thermocouple and controlled within ± 1 K by hot air and/or cooled dry nitrogen gas from liquid nitrogen. The Raman spectrum of glassy solution M2 was measured by immersing the sample tube into liquid nitrogen (77 K).

2.4 X-ray Diffraction Measurements and Data Treatment

X-ray diffraction measurements were performed on solution M2 at 243 and 298 K, on solution D2(1) at 298 K, and on solution D2(2) at 243 K with a Rigaku $\theta-\theta$ type diffractometer using Mo$K\alpha$ radiation ($\lambda = 71.07$ pm). A LiF (200) crystal was used for monochromatization of the scattered X-ray radiation. The observed range of the scattering angle (2θ) was from 2° to 140°, corresponding to the scattering vector $s\,(=4\pi\sin\theta/\lambda)$ of 3.1×10^{-3} to 0.166 pm^{-1}. The measurements were repeated twice over the whole angle range. Different slit combinations and step angles were used depending on the angle range. The total count per data point was 20000 for solution M2 at 243 and 298 K and solution D2(2) at 243 K, and 40000 for solution D2(1) at 298 K. The details of the X-ray diffractometer and measurements have been described in [12, 13]. The temperature of the sample solutions was measured with a copper-constantan thermocouple and controlled within ± 0.2 K [5]. The measured X-ray intensities, $I(s)$, were corrected for background, absorption, and polarization in the usual way [14]. The corrected intensities were then normalized to electron units by the conventional methods [15–17] and further corrected for the incoherent scattering and the double scattering [14]. The structure function, $i(s)$, is given as

$$i(s) = I^{\mathrm{coh}}(s) - \sum_i x_i f_i^2(s), \tag{3}$$

where $f_i(s)$ represents the atomic scattering factor of atom i corrected for the anomalous dispersion. The s-weighted structure function is Fourier transformed into the radial distribution function $D(r)$ as

$$D(r) = 4\pi r^2 \varrho_0 + \frac{2r}{\pi}\int_0^{s_{\max}} s\,i(s)\,M(s)\sin(rs)\,\mathrm{d}s. \tag{4}$$

Here, $\varrho_0\,(=[\Sigma x_i f_i(0)]^2/V)$ stands for the average scattering density of a sample solution, $s_{\max}$ is the maximum s-value attained in the measurements ($s_{\max} = 0.161$ pm^{-1} for solution M2 and 0.166 pm^{-1} for solutions D2(1) and D2(2)). A modification function $M(s)$ of the form $[\Sigma x_i f_i^2(0)/\Sigma x_i f_i^2(s)]\exp(-100\,s^2)$ was used.

A comparison between the experimental structure function and the theoretical one based on a model was made by a least-squares refinement procedure of minimizing the error square sum,

$$U = \sum_{s_{\min}}^{s_{\max}} s^2\{i(s)_{\mathrm{exp}} - i(s)_{\mathrm{calcd}}\}^2. \tag{5}$$

The theoretical intensities $i(s)_{\mathrm{calcd}}$ were calculated by

$$\begin{aligned} i(s)_{\mathrm{calcd}} = &\sum_{i}\sum_{\substack{j\\ i\neq j}} x_i n_{ij} f_i(s) f_j(s)\frac{\sin(r_{ij}s)}{r_{ij}s}\exp(-b_{ij}s^2) \\ &-\sum_{i}\sum_{\substack{j\\ i\neq j}} x_i x_i f_i(s) f_j(s) \\ &\cdot\frac{4\pi R_j^3}{V}\,\frac{\sin(R_j s) - R_j s\cos(R_j s)}{R_j s^3}\exp(-B_j s^2). \end{aligned} \tag{6}$$

The first term of the right-hand-side of (6) is related to the short-range interaction characterized by the interatomic distance r_{ij}, the temperature factor b_{ij}, and the number of interactions n_{ij} for atom pair i–j. The second term arises from the interaction between a spherical hole and the continuum electron distribution beyond this discrete distance. R_j is the radius of the spherical hole around the j-th atom and B_j is the softness parameter for emergence of the continuum electron distribution.

All treatments of the X-ray diffraction data were carried out with the programs KURVLR [14] and NLPLSQ [18].

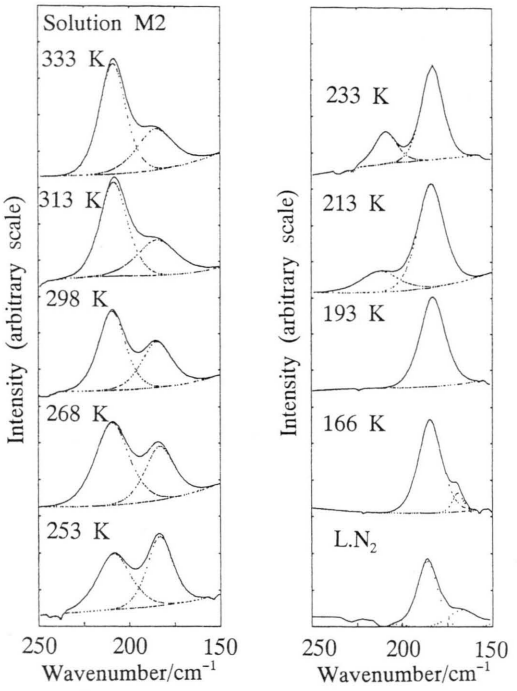

Fig. 1. Raman spectra for zinc(II) bromide methanol solution M2 at various temperatures. The spectra at 166 K and liquid nitrogen temperature correspond to the supercooled and glassy solutions, respectively. The solid lines represent the observed intensities, and the dots show the components obtained by the least-squares fits.

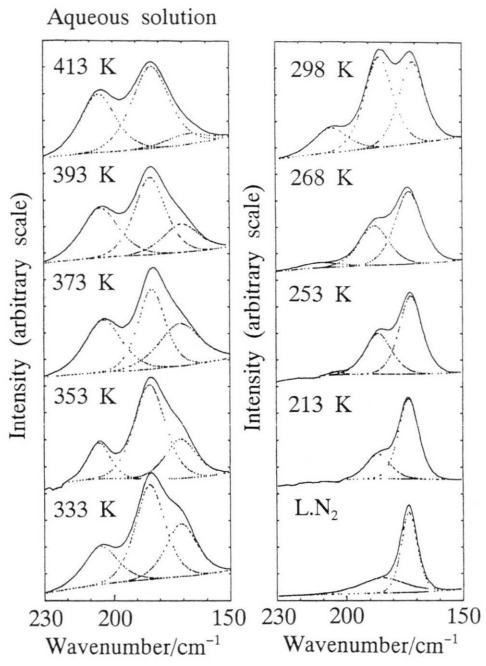

Fig. 2. Raman spectra for aqueous zinc(II) bromide solution with $[H_2O]/[ZnBr_2] = 10$ at various temperatures [6, 7]. The spectra below 268 K and liquid nitrogen temperature correspond to the supercooled and glassy solutions. The solid line represents the observed intensities and the dots show the components obtained by the least-squares fits.

3. Results and Discussion

3.1 Raman Spectra

Raman spectra of the methanol and DMF solutions M2 and D2(1) at various temperatures are shown by solid lines in Figs. 1 and 3, respectively. For comparison Raman spectra of an aqueous zinc(II) bromide with the $[H_2O]/[ZnBr_2]$ molar ratio of 10 in [6, 7] are also shown in Figure 2. The observed Raman bands were deconvoluted by a nonlinear least-squares method using a Lorentzian-Gaussian function expressed by

$$I(\nu) = I(\nu_0)\,[\exp\{-4\ln 2\,((\nu-\nu_0)/\sigma)^2\} \cdot \{1+(\nu-\nu_0)/\sigma\}^{-1}]^{1/2}, \quad (7)$$

where $I(\nu_0)$ denotes the peak height at the peak position ν_0, and σ is the half width of the peak. The parameters $I(\nu_0)$, ν_0, and σ were allowed to vary independently in the optimizing process. The resolved components and the background are shown by dots in Figs. 1, 2, and 3.

As seen in Fig. 1, two Raman bands are observed at 209 and 184 cm^{-1} for solution M2 at 298 K. On the basis of the assignments of the bands observed for the aqueous solutions in Fig. 2 [6, 7], the bands at 209 and 184 cm^{-1} for the methanol solution are ascribable to the ν_1 mode of the symmetric Zn–Br vibration within the dibromo- and tribromozinc(II) complexes, respectively. It should be noted that the peak positions of the ν_1 mode for the dichloro-, trichloro-, and tetrachlorozinc(II) complexes are not significantly altered between water [19] and alcohols [20]. It is interesting that no ν_1 band for the tetrabromo species is observed in the methanol solution at ambient temperature, in contrast to the aqueous system.

With lowering temperature, the intensity of the ν_1 band for the dibromo complex decreases gradually, accompanied by an increase of the ν_1 band for the tribromo complex. A comparison between Raman

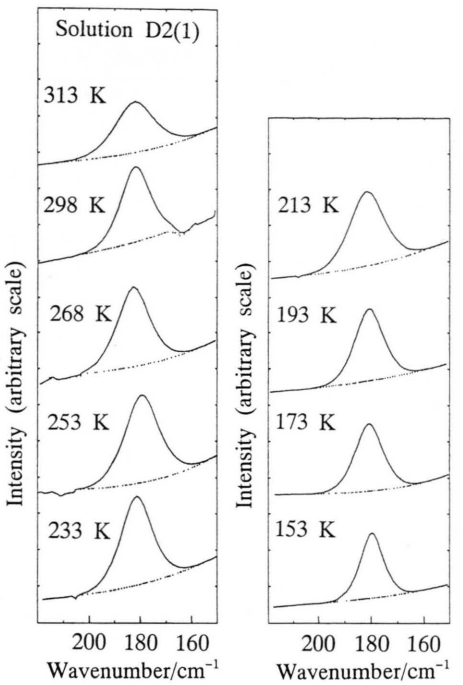

Fig. 3. Raman spectra for the zinc(II) bromide DMF solution D2(1) at various temperatures. The three spectra below 193 K correspond to the supercooled solutions. The solid lines represent the observed intensities and the dots show the components obtained by the least-squares fits.

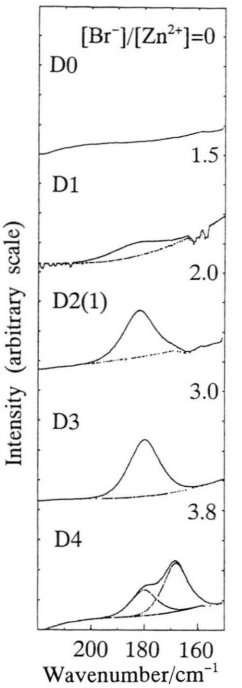

Fig. 4. Raman spectra for the zinc(II) bromide DMF solutions D0, D1, D2(1), D3, and D4 with the $[Br^-]/[Zn^{2+}]$ molar ratios of 0, 1.5, 2.0, 3.0, and 3.8, respectively, at 298 K. The solid line represents the observed intensities and the dots show the components obtained by the least-squares fits.

spectra of the methanol and aqueous solutions measured at the same temperature shows that the formation of higher complexes is not so favored in the methanol solution as in the aqueous solution. The ν_1 band for the tetrabromo species is observable at 169 cm^{-1} only at temperatures as low as 166 K and liquid nitrogen temperature (77 K) in supercooled and glassy solutions.

Raman spectra for the DMF solution D2(1) at various temperatures are shown in Figure 3. The spectra below 193 K correspond to the supercooled DMF solution. As seen in Fig. 3, only one Raman band is observed at 181 cm^{-1}, and it does not change in intensity with temperature, in marked contrast with those for the methanol and aqueous solutions (Figs. 1 and 2). In order to further examine the Raman bands of the species in the DMF solution, Raman spectra were also recorded at 298 K for the solutions D0, D1, D3, and D4 with various $[Br^-]/[Zn^{2+}]$ molar ratios (Fig. 4) together with the spectrum for solution D2(1) with the ratio of 2.0. As seen in Fig. 4, one Raman band is observed at 181 cm^{-1} for solutions D1, D2(1), and D3. However, another Raman band appears at 168 cm^{-1} at the high $[Br^-]/[Zn^{2+}]$ ratio of 3.8. The Raman bands at 181 and 168 cm^{-1} of the DMF solutions are assigned to the ν_1 (Zn–Br) mode of the tribromo- and tetrabromozinc(II) complexes, respectively, as in the methanol and aqueous solutions. A calorimetric study on the formation of the zinc(II) bromo complexes in DMF [21] revealed that the dibromo complex is also formed at $[Br^-]/[Zn^{2+}] = 2$. It is thus likely that the 181 cm^{-1} band includes in part that of the dibromo complex.

This shift of the ν_1 band toward lower frequency for the dibromo species from the methanol to DMF solutions may be ascribed to the donicity of the solvent. X-ray and calorimetric investigations on aqueous and DMF solutions of zinc(II) bromide [21, 22] have shown that the dibromo complex has a tetrahedral coordination of $[ZnBr_2(solvent)_2]$ in both solutions.

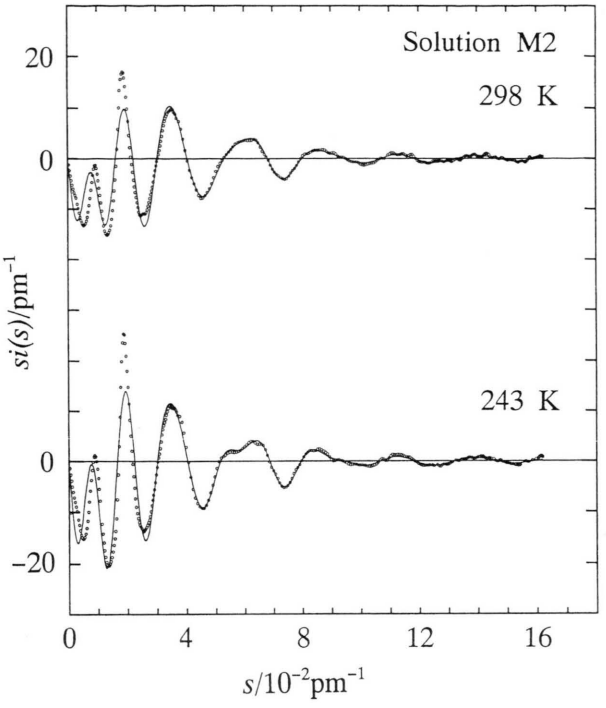

Fig. 5. Structure functions $i(s)$ multiplied by s for the zinc(II) bromide methanol solution M2 at 243 and 298 K. The experimental values are shown by circles and those calculated with the parameters given in Tables 2 and 3 by the solid lines.

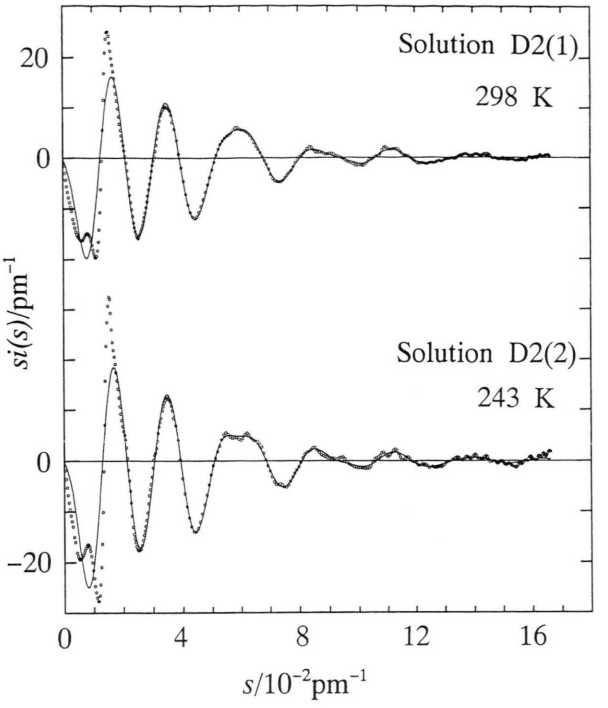

Fig. 6. Structure functions $i(s)$ multiplied by s for the zinc(II) bromide DMF solutions D2(1) and D2(2) at 298 and 243 K, respectively. The experimental values are shown by circles and those calculated with the parameters given in Tables 2 and 4 by the solid lines.

This would also be the case in the methanol solution. The donor number DN, which is an indication of the donicity of solvent, is 26.6 for DMF, which is the largest among the three solvents (18.0 for water and 19.0 for methanol). The Zn–Br bonds within the dibromo complex are probably weakened in the order of DMF < methanol ≈ water by electron donation from solvent oxygen atoms to the zinc(II) ion. Consequently, the ν_1 Raman band for the dibromo complex will shift to a lower frequency in the DMF solution, whereas a small shift is expected for the aqueous and methanol solutions. The tribromo complex also has a tetrahedral coordination in these solutions. The strength of Zn–Br bonds within the tribromo complex may be less affected by electron donation from the solvents because only one solvent binds to the zinc(II) ion and, in addition, the strength of Zn–O bond within the tribromo complex is more weakened than that within the dibromo species [5–7]. Thus the ν_1 band for the tribromo complex will not be affected significantly by the solvents. As shown in Fig. 3, Raman spectra for the DMF solution at various temperatures suggest that the dibromo and tribromo complexes are formed preferentially, while the tetrabromo complex is not formed in the used temperature range.

3.2 X-ray Scattering

Figures 5 and 6 shows the s-weighted structure functions for the methanol and DMF solutions M2, D2(1), and D2(2) at 243 and 298 K. The corresponding total radial distribution functions (RDFs) in the form of $D(r) - 4\pi r^2 \varrho_0$ are shown in Figs. 7 and 8.

As seen in Fig. 7, the peaks and shoulders are observed at 140, 236, 360, 400, 490, and 600–900 pm for the methanol solution at 243 and 298 K. The first peak at 140 pm is ascribable to the O–H, C–H, C–O bonds, and nonbonding H···H interactions within a methanol molecule [23]. The second peak at 236 pm arises mainly from the Zn–Br interactions within the zinc(II) bromo complexes present in the

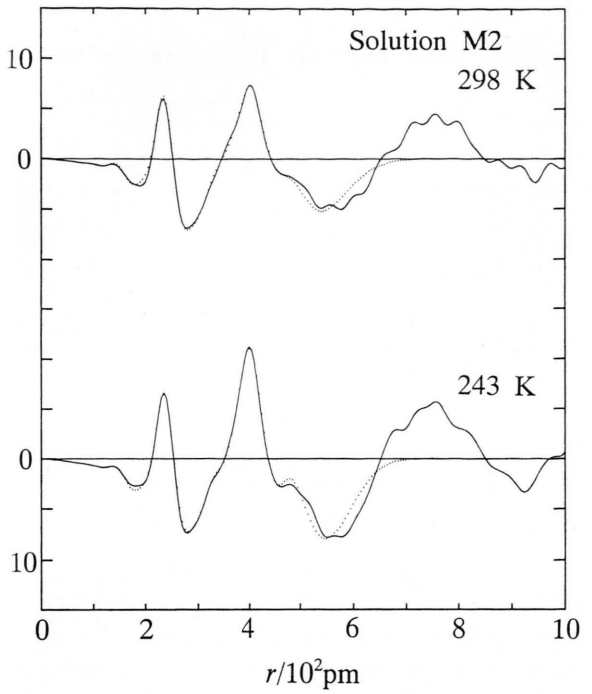

Fig. 7. Radial distribution functions $D(r) - 4\pi r^2 \varrho_0$ for the zinc(II) bromide methanol solution M2 at 243 and 298 K. Experimental (solid lines) and calculated (dots).

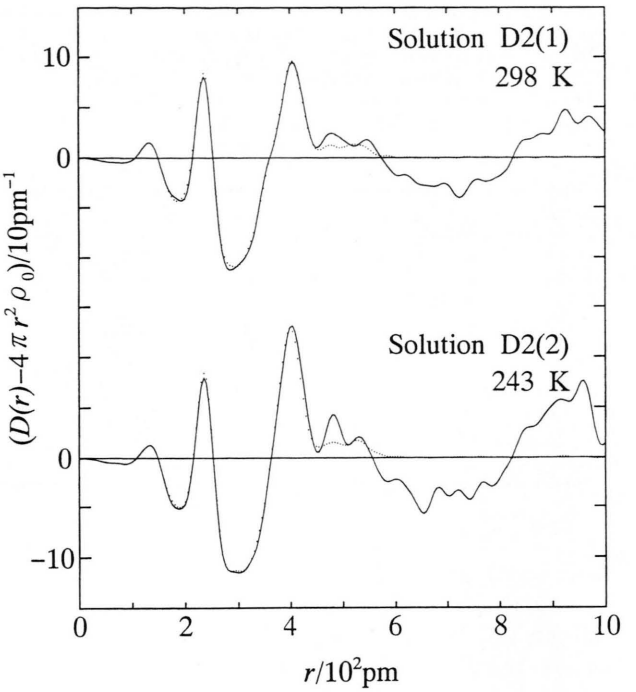

Fig. 8. Radial distribution functions $D(r) - 4\pi r^2 \varrho_0$ for the zinc(II) bromide DMF solutions D2(1) and D2(2) at 298 and 243 K, respectively. Experimental (solid lines) and calculated (dots).

solution. This peak also includes a contribution of the $Zn-O(CH_3OH)$ interactions within the zinc(II) methanol solvate complex and the lower species such as the monobromo- and dibromo complexes which should appear around 200 ~ 210 pm [6, 7, 22]. Furthermore, the nonbonding $O \cdots H$ and $C \cdots H$ interactions within a methanol molecule contribute to the peak [23].

The distinct peak at 400 pm is assigned mainly to the nonbonding $Br \cdots Br$ interactions within the tetrahedral zinc(II) bromo complexes, because the ratio (~1.69) of the $Br \cdots Br$ to the Zn–Br peak positions is close to 1.63, an expected value for a tetrahedral coordination. A shoulder around 360 pm is probably due to the nonbonding $Br \cdots O(CH_3OH)$ interactions within the dibromo- and tribromozinc(II) complexes. In addition, it has been suggested from the crystal structure of $KZnBr_3 \cdot 2H_2O$ [24] that within 300 ~ 500 pm there exist H_2O-H_2O and $Br-H_2O$ hydrogen bonds in the first and second shells and several interactions between a zinc(II) ion and water molecules in the second shell in aqueous solutions [6, 7]. This is also the case for the methanol solution, in which hydrogen bonds are present between CH_3OH-CH_3OH and $Br-CH_3OH$ in the range of 280–490 pm of the RDFs. The broad peak at 600–900 pm, which may originate from various long-range interactions in the solution, was not taken account of and an even electron distribution was assumed.

As is clearly seen in Fig. 7, when the temperature is lowered, the first Zn–Br peak does not seem to change significantly, while the second $Br \cdots Br$ peak becomes larger and sharper, accompanied by a decreasing $Br \cdots O$ shoulder.

In the RDFs (Fig. 8) for the DMF solution at 243 and 298 K, three distinct peaks are observed at 140, 239, and 400 pm. The first peak at 140 pm is attributed to C–H, C–N, and C=O bonds within a DMF molecule [10]. The second and third peak positions agree with those observed for the aqueous [6, 7, 22] and methanol solutions (Figure 7). According to the crystal structures of $Zn(ClO_4)_2 \cdot (dmf)_6$ [25] and

Table 2. Optimized parameters of the interactions within the zinc(II) bromide complexes for the sample solutions at various temperatures: the interatomic distance r (pm), the temperature factor b (pm^2), the number of interactions n per zinc(II) ion. The values in parentheses are standard deviations estimated from the least-squares refinements. The parameters without standard deviations were fixed during the calculations. [a] [7].

Interaction	Parameter	Solution M2		Solutions D2(2) and D2(1)		Aqueous solution[a]	
		243 K	298 K	243 K	298 K	233 K	298 K
Zn–O	r	210	207	216	210	210	210
	$b/10$	2	2	1.5	1.5	5	5
	n	2.6	2.3	2.5	2.1	3.0	2.5
Zn–Br	r	236.6(2)	235.3(2)	237.8(3)	237.1(1)	239.4(2)	238.2(1)
	$b/10$	2	2	1.5	1.5	2	2
	n	1.98(2)	1.93(3)	2.06(4)	2.03(2)	2.03(2)	1.97(2)
Br···Br	r	398.8(6)	401.5(6)	398.2(6)	402.3(4)	390.3(4)	391.3(4)
	$b/10$	20	20	8	8	20	20
	n	1.94(6)	1.52(5)	1.8	1.32(3)	2.41(5)	1.88(4)
Br···O	r	360	360	360	360	360	360
	$b/10$	20	20	8	8	10	10
	n	2.2	3.0	2.5	3.4	0.70	2.0

$ZnCl_2(dmf)_2$ [26] and of calorimetric and potentiometric data on zinc(II) halogeno complexes in organic solvents [27, 28], the zinc(II) DMF hexa solvate has an octahedral coordination, and the dibromo-, tribromo-, tetrabromozinc(II) complexes have a tetrahedral one in their DMF solutions as found in aqueous solutions [22]. From these considerations, the second peak at 239 pm is mainly assigned to the Zn–Br interactions within the zinc(II) bromo complexes. Furthermore, the peak includes those for the Zn–O(dmf) interactions within the zinc(II) DMF solvates, and the lower species and for the nonbonding C···C, C···O, and N···O interactions within a DMF molecule [10].

The third peak at 400 pm is mainly ascribed to the nonbonding Br···Br interactions within the tetrahedral zinc(II) bromo complexes. The nonbonding Br···O(dmf) interactions within the dibromo- and tribromocomplexes are observable as a shoulder around 360 pm in the RDF at 298 K. Two broad peaks at 450–650 and 800–1000 pm should be attributed to complicated medium- and long-range interactions in the solution, which were not analyzed in the present study, except for nonbonding Zn···(dmf) interactions at 528 pm, and an even electron distribution was assumed in the subsequent analysis.

As seen in Fig. 8, when the DMF solution is cooled down, the second Br···Br peak becomes larger and sharper, and the shoulder peak Br···O diminishes, although the first Zn–Br peak does not change significantly. This trend is similar to that found for the aqueous [6, 7] and the present methanol solutions (Figure 7).

In order to refine the structure parameters of the zinc(II) bromo complexes in both methanol and DMF solutions, a least-squares method was applied to the structure functions over the scattering vector of $0.1 \times 10^{-2} < s/pm^{-1} < 0.16$. The interatomic distance r, the temperature factor b, the number of interactions n, and the parameters R and B for a continuum electron distribution in (6) were treated as variables in the course of refinements. The structure parameters for methanol and DMF molecules were fixed at the values obtained from a neutron scattering experiment on liquid CD_3OD [23] and an X-ray diffraction study on pure DMF [10]. The nonbonding interactions between a zinc(II) ion and all atoms within DMF molecules in the first shell were taken into account in the analysis, where the bond length and angle were assumed as Zn–O = 210 pm and $\angle$ Zn–O–C = 120°, respectively.

The optimized parameter values within the first coordination shell are summarized in Table 2, together with those obtained for an aqueous zinc(II) bromide solution with $[H_2O]/[ZnBr_2] = 5$ at 233 and 298 K in [7]. The structure parameters of important medium range interactions and of a continuum electron distribution are listed in Tables 3 and 4 for the methanol and DMF solutions, respectively.

Figures 5, 6, 7, and 8 show that the theoretical $si(s)$ and RDF calculated by using the optimized parameter values in Tables 2–4 reproduced well the observed ones except the long-range interactions not taken into account in the present analysis.

Table 3. Optimized parameters of the medium-range interactions and of the continuum electron distribution for the solution M2 at 243 and 298 K: the interatomic distance r (pm), the temperature factor b (pm^2), the number of interactions n per zinc(II) ion, and parameters for the continuum electron distribution R (pm) and B (pm^2). The values in parentheses are standard deviations estimated from the least-squares refinements. The parameters without standard deviations were fixed during the calculations.

Interaction	Parameter	243 K	298 K
O···O	r	280	280
	$b/10$	25	20
	n	0.35	0.55
Zn···O	r	397	400
	$b/10$	25	25
	n	17	9.9
Br···O	r	330	333
	$b/10$	20	25
	n	8.5	6.6
Zn···O	r	480	489
	$b/10$	25	20
	n	13	6.0
Br···O	r	419	450
	$b/10$	25	20
	n	4.3	4.5
Zn	R	321 (20)	323
	$B/10$	50	100
Br	R	586 (3)	560 (3)
	$B/10$	80	137 (25)
H	R	428 (18)	341 (14)
	$B/10$	35	100
C	R	469 (11)	427
	$B/10$	50	300
O	R	263 (8)	303 (7)
	$B/10$	50	10

Table 4. The structure parameters of the nonbonding interactions between a central zinc(II) ion and the atoms in the solvating DMF molecules for solutions D2(1) and D2(2) at 298 and 243 K, respectively: the interatomic distance r (pm), the temperature factor b (pm^2), the number of interactions n per zinc(II) ion, and optimized parameters for the continuum electron distribution R (pm) and B (pm^2). The values in parentheses are standard deviations estimated from the least-squares refinements. The parameters without standard deviations were fixed during the calculations.

Interaction	Parameter	Solution D2(2)	Solution D2(1)
		243 K	298 K
Zn···C	r	292	292
	$b/10$	10	10
	n	2.5	2.1
Zn···N	r	421	421
	$b/10$	10	10
	n	2.5	2.1
Zn···C	r	473	473
	$b/10$	10	10
	n	2.5	2.1
Zn···C	r	528	528
	$b/10$	10	10
	n	2.5	2.1
Zn	R	365	310
	$B/10$	1	50
Br	R	361	369 (5)
	$B/10$	1	1
H	R	313	325
	$B/10$	15	1
C	R	282 (7)	313 (3)
	$B/10$	1	54
N	R	321 (31)	296
	$B/10$	1	25
O	R	347 (17)	316
	$B/10$	1	100

As seen in Table 2, the number of Zn–Br interactions, which corresponds to the average coordination number of one zinc(II) ion for bromide ions, does not significantly change with temperature and is $n_{Zn-Br} \approx 2$ for both methanol and DMF solutions as well as for the aqueous solution. On the contrary, the number of nonbonding Br···Br interactions for the methanol solution increases from 1.52(5) at 298 K to 1.94(6) at 243 K. The difference between the $n_{Br\cdots Br}$ values at the two temperatures is 0.42, beyond estimated uncertainties in the present analysis.

In the refinement of the parameters for the DMF solution at 243 K, the value of $n_{Br\cdots Br}$ could not be treated as a variable because of overlapping of medium-range interactions (450–650 pm) reinforced at low temperature. When $n_{Br\cdots Br}$ was fixed at 1.8, the peak at 400 pm could be reproduced best as seen by dots in Fig. 8. It is thus concluded that the $n_{Br\cdots Br}$ value for the DMF solution also increases from 1.32(3) at 298 K to 1.8 at 243 K. The increase in the $n_{Br\cdots Br}$ value suggests that the Br^- richer complex is formed favorably at low temperatures in both methanol and DMF solutions. However, the $n_{Br\cdots Br}$ values for the methanol (1.94) and DMF solution (1.8) at 243 K are much smaller than that (2.41) for the aqueous solution at 233 K, showing that the tribromo complex is mainly formed and the tetrabromo complex is less favored in both methanol and DMF solutions than in the aqueous solution at low temperature. Furthermore, the "lowest" complex $[Zn(solvent)_6]^{2+}$ in the series of the zinc(II) bromo complexes should also be formed in both solutions at low temperature because of no significant change in the average coordination number n_{Zn-Br} with temperature, as found in the corresponding supercooled and glassy aqueous solutions [7].

The above discussion on equilibrium shifts with decreasing temperature is well supported by other struc-

ture parameters as follows. The Zn–Br distance for the zinc(II) bromo complexes slightly increases from 235.3(2) at 298 K to 236.6(2) pm at 243 K in the methanol solution and from 237.1(1) at 298 K to 237.8(3) pm at 243 K in the DMF solution. On the other hand, the distance of the nonbonding Br···Br interactions decreases slightly; 401.5(6) at 298 K to 398.8(6) pm at 243 K in the methanol solution and 402.3(4) at 298 K to 398.2(6) pm at 243 K in the DMF solution. The Br···Br distances in the methanol and DMF solutions at both temperatures are significantly longer than that (390.3(4) pm) in the aqueous solution at 233 K, in which the tetrabromo complex is mainly formed. An average Br–Zn–Br bonding angle within the zinc(II) bromo complexes in the solutions was calculated by using the values of the Zn–Br and Br···Br distances. When the temperature is lowered, the bonding angle decreases slightly; 117° at 298 K to 114° at 243 K in the methanol solution and 116° at 298 K to 114° at 243 K in the DMF solution. However, the Br–Zn–Br angles for both solutions at 243 K are larger than that (109°) for the aqueous solutions at 233 K. According to structure parameters of the individual zinc(II) bromo complex in aqueous solution at ambient temperature determined by Goggin et al. [22] by X-ray diffraction, the Zn–Br and Br···Br distances and the average Br–Zn–Br angle are 238.6 pm, 401 pm, and 114°, respectively, for the dibromo complex, 238.6 pm, 400 pm, and 114°, respectively, for the tribromo complex, and 240.8 pm, 393 pm, and 109°, respectively, for the tetrabromo complex. The Br···Br distance seems to decrease slightly from the dibromo to the tribromo complexes in aqueous solution. A similar decrease in the Br···Br distance is observed for both methanol and DMF solutions with decreasing temperature. Moreover, from a comparison between the structure parameters determined for the methanol and DMF solutions and those for the individual complexes obtained by Goggin et al., the average structure of the zinc(II) bromo complexes in the present methanol and DMF solutions at 243 K is close to that of the tribromo complex. Considering the above changes in the Zn–Br distances and Br–Zn–Br bond angle with temperature, it is again concluded that the formation of the tribromo complex is promoted in both methanol and DMF solutions with decreasing temperature, whereas the dibromo complex is formed as the predominant species at ambient temperature.

These X-ray results for the methanol solution are consistent with the conclusion from the present Raman spectroscopic measurements. In spite of no change in Raman spectra for the DMF solution with temperature (Fig. 3), the X-ray results have revealed that the amount of the tribromo complex increases in the DMF solution at the low temperature.

3.3 Equilibrium Shifts

The present Raman and X-ray scattering data have demonstrated that both equilibria (8) and (9) shift to the right-hand-side in the methanol solution with lowering temperature, but less favorably than in aqueous solutions. In the DMF solution, only the equilibrium shift (8) takes place with decreasing temperature, and no tetrabromo species is formed even at liquid-nitrogen temperature:

$$3\,[ZnBr_2(solv)_2] + 2\,solv = 2\,[ZnBr_3(solv)]^- + [Zn(solv)_6]^{2+}, \quad (8)$$

$$4\,[ZnBr_3(solv)]^- + 2\,solv = 3\,[ZnBr_4]^{2-} + [Zn(solv)_6]^{2+}. \quad (9)$$

The solvent dependence on equilibrium shifts (8) and (9) is now discussed. The hydrogen-bonds between methanol molecules will be strengthened in the supercooled and glassy solutions as is seen in aqueous solutions [6–9]. However, the amount of hydrogen-bonds in the methanol solution is smaller than that in the aqueous solution; hence, methanol molecules expelled from the first coordination shell of the dibromo and tribromo complexes will be less stabilized at low temperatures than in the aqueous solution; thus the formation of the "higher" complexes like the tetrabromo species is suppressed in the methanol solution. At high temperatures, the hydrogen-bonds between methanol molecules will be broken, and methanol molecules will move more freely than water molecules; thus methanol molecules will bind more easily to a zinc(II) ion to form the dibromo complex than in the aqueous system.

On the other hand, the intermolecular interaction in the DMF solution is of the dipole–dipole and van der Waals type and much weaker than that in the aqueous and methanol solutions, as has been reported in the X-ray study [10, 11]; hence no temperature effect comparable with that for the aqueous and methanol solutions is expected on the equilibria.

However, considering the fact that pure DMF freezes at 212 K, the motion of DMF molecules will be retarded at low temperatures. Thus, a DMF molecule expelled from the first coordination shell of the dibromo complex will be slightly stabilized in the DMF solution at low temperature, and the tribromo complex tends to be formed at low temperature. The tetrabromo complex is not formed, however.

The thermodynamic parameters [21, 29] support the above discussion on the difference of the equilibria between the DMF and aqueous solutions. To our knowledge, no reliable thermodynamic data are available for the methanol solution of zinc(II) bromide. Shchukarev et al. [29] determined the stepwise enthalpies in aqueous solution from the stability constants measured at different temperatures; ΔH_n° at 298 K are 0, 0, 110, and -110 kJ mol^{-1} for $n = 1$, 2, 3, and 4, respectively. In the DMF solution, on the other hand, the stepwise thermodynamic parameters have been determined by titration calorimetry at 298 K by Ishiguro et al. [21]. The enthalpies at 298 K are 33, 4.0, and -5.6 kJ mol^{-1} for $n = 1$, 2, and 3, respectively. It is reported that the forth complex is not formed in DMF solution. In aqueous solution the enthalpy for the fourth step is largely negative, while those for the other steps are zero or positive. The third step in the DMF solution is exothermic, but its value is less negative than that for the fourth step in aqueous solution. It would be expected, therefore, that with decreasing temperature the amount of the tetrabromo complex increases in aqueous solution and that the formation of the tribromo complex becomes slightly favorable in DMF solution. The positive value of ΔH_1° for the DMF solution suggests that at low temperature the "lowest" complex, $[Zn(solv)_6]^{2+}$, is more favored in DMF than in aqueous solution. This tendency will be attributed to the larger donicity of the DMF molecule (DN = 26.6) than that of the water molecule (DN = 18.0).

4. Concluding Remarks

The combined Raman and X-ray scattering study of the methanol and DMF solutions of zinc(II) bromide at various temperatures has revealed the equilibria of the individual zinc(II) bromo complexes and their average structures in the two solutions. Together with the previous findings of the corresponding aqueous solution, it has been found that at low temperatures the tetrabromo complex is formed most favorably in aqueous solution and less favorably in the methanol solution. In the DMF solution no tetrabromo complex is formed even at liquid-nitrogen temperature. These trends in the equilibria with temperature have been interpreted in terms of temperature dependent ion–solvent and solvent–solvent interactions.

Acknowledgements

We thank Prof. Mitsuru Tanaka for letting us use a densitometer, and Gohki Sadakuni and Shin-ichiro Matsukuma for their help in Raman spectral measurements. All calculations were performed at the Computer Center for Fukuoka University. The present work was supported in part by the Grant-in-Aid for Scientific Research (No. 6453029) from the Ministry of Education, Science, and Culture of Japan.

[1] M. Nomura and T. Yamaguchi, J. Phys. Colloq. C8 **47** (Suppl. 12), 619 (1986).
[2] M. Nomura and T. Yamaguchi, J. Phys. Chem. **92,** 6157 (1988).
[3] T. Yamaguchi, M. Nomura, H. Wakita, and H. Ohtaki, J. Chem. Phys. **89,** 5153 (1988).
[4] T. Yamaguchi, Pure Appl. Chem. **62,** 2251 (1990).
[5] T. Takamuku, T. Yamaguchi, and H. Wakita, J. Phys. Chem. **95,** 10098 (1991).
[6] T. Takamuku, M. Ihara, T. Yamaguchi, and H. Wakita, Z. Naturforsch. **47a,** 485 (1992).
[7] T. Takamuku, K. Yoshikai, T. Yamaguchi, and H. Wakita, Z. Naturforsch. **47a,** 841 (1992).
[8] K. Yamanaka, M. Yamagami, T. Takamuku, T. Yamaguchi, and H. Wakita, J. Phys. Chem. **97,** 10835 (1993).
[9] M. Yamagami, T. Yamaguchi, and H. Wakita, J. Chem. Phys. **100,** 3122 (1994).
[10] H. Ohtaki, S. Itoh, T. Yamaguchi, S. Ishiguro, and B. M. Rode, Bull. Chem. Soc. Japan **56,** 3460 (1983).
[11] H. Ohtaki, S. Itoh, and B. M. Rode, Bull. Chem. Soc. Japan **59,** 271 (1986).
[12] H. Wakita, M. Ichihashi, T. Mibuchi, and I. Masuda, Bull. Chem. Soc. Japan **55,** 817 (1982).
[13] T. Yamaguchi, G. Johansson, B. Holmberg, M. Maeda, and H. Ohtaki, Acta Chem. Scand. **A 38,** 437 (1984).
[14] G. Johansson and M. Sandström, Chem. Scrip. **4,** 195 (1973).
[15] K. Furukawa, Rep. Progr. Phys. **25,** 395 (1962).
[16] J. Krogh-Moe, Acta Crystallogr. **2,** 951 (1956).
[17] N. Norman, Acta Crystallogr. **10,** 370 (1957).
[18] T. Yamaguchi, Doctoral Thesis, Tokyo Institute of Technology, 1978.
[19] H. Kanno and J. Hiraishi, J. Raman Spectrosc. **9,** 85 (1980).

[20] H. Kanno and S. Yamauchi, J. Solution Chem. **20,** 589 (1991).
[21] S. Ishiguro, M. Miyauchi, and K. Ozutsumi, J. Chem. Soc. Dalton Trans. **1990,** 2035.
[22] P. L. Goggin, G. Johansson, M. Maeda, and H. Wakita, Acta Chem. Scand. **A 38,** 625 (1984).
[23] Y. Tanaka, N. Ohtomo, and K. Arakawa, Bull. Chem. Soc. Japan **57,** 644 (1984).
[24] R. Holinski and B. Brehler, Acta Crystallogr. **B 26,** 1915 (1970).
[25] W. Schneider, Helv. Chim. Acta **46,** 1842 (1963).
[26] H. Suzuki, N. Fukushima, S. Ishiguro, H. Masuda, and H. Ohtaki, Acta Crystallogr. **C 47,** 1838 (1991).
[27] S. Ishiguro, K. Ozutsumi, and H. Ohtaki, Bull. Chem. Soc. Japan **60,** 531 (1987).
[28] (a) S. Ahrland and N.-O. Björk, Acta Chem. Scand. **A 30,** 265 (1976); (b) S. Ahrland and N.-O. Björk, and R. Portanova, Acta Chem. Scand. **A 30,** 270 (1976).
[29] S. A. Shchukarev, L. S. Lilich, and V. A. Latysheva, Zh. Neorg. Khim. **1,** 225 (1956).